ELSEVIER

Materials Science and Engineering A 454–455 (2007) 104–113

MATERIALS SCIENCE & ENGINEERING A

www.elsevier.com/locate/msea

Infrared vacuum brazing of Ti–6Al–4V and Nb using the Ti–15Cu–15Ni foil

D.W. Liaw [a], Z.Y. Wu [b], R.K. Shiue [b,*], C.S. Chang [c]

[a] *Department of Materials Science and Engineering, National Dong Hwa University, Hualien 974, Taiwan*
[b] *Department of Materials Science and Engineering, National Taiwan University, Taipei 106, Taiwan*
[c] *Engineered Materials Solutions, 39 Perry Avenue, MS 4-1, Attleboro, MA 02703-2410, USA*

Received 9 September 2006; received in revised form 29 October 2006; accepted 10 November 2006

Abstract

The microstructural evolution of infrared brazed joint is primarily depended upon redistribution of alloying elements such as Cu, Ni and Nb across the joint. For the specimen infrared brazed at 970 °C for 180 s, the joint primarily consists of coarse eutectic Ti_2Cu, Ti_2Ni intermetallics and transformed β-Ti. Increasing the brazing time to 600 s results in a fine eutectoid microstructure dominating the entire joint due to the depletion of Cu and Ni from the braze alloy into Ti–6Al–4V substrate. Ti_2Cu, Ti_2Ni and transformed β phases are almost absent from the specimen infrared brazed for 3600 s, and the β-Ti is stabilized by alloying high concentration of Nb. Based on the shear test result, all cracks propagate along the Nb substrate with typical ductile dimple rupture appearance. Consequently, Ti–6Al–4V and Nb can be vacuum brazed by Ti–15Cu–15Ni foil with good joint strength.

Keywords: Infrared brazing; Ti–15Cu–15Ni; Nb; Phase diagram; Microstructure

1. Introduction

The importance of Ti alloys is increasing in the past decade due to structural demanding from aerospace applications [1,2]. Ti–6Al–4V is a type of α–β titanium alloys, which can be strengthened by solution and aging heat treatments. The Nb metal belongs to refractory metals with the melting point of 2468 °C [3]. It has been applied for its corrosion resistance in chemical and nuclear applications or for its low density and high melting point in aerospace and propulsion applications. Accordingly, joining of Ti–6Al–4V and Nb has potential applications in industry.

Ag-based braze alloys are featured with low melting points, and they have been successfully applied in brazing Ti–6Al–4V and Nb metal in the previous study [4]. However, many Ag-based braze alloys are suffered from insufficient oxidation resistance and low creep strength [5–8]. It has been reported that Ti–6Al–4V and Nb are vacuum brazed using the Ti-based braze alloys [9,10]. The Ti-based braze alloy provides an alternative approach in brazing the Nb and Ti alloy. A cold roll-bonding process is applied to combine Ti, Cu and Ni strips into a layered composite that allows conventional cold rolling process to produce the clad Ti–15Cu–15Ni brazing foil studied here [11,12].

The development of high-intensity quartz lamps and the availability of suitable reflectors have made infrared heating an important generator of heat for brazing [13]. Compared with the conventional furnace brazing, infrared brazing is featured with an extraordinary heating rate as high as 50 °C/s [12–15]. The microstructural evolution of the joint, especially for the very early stage of brazing, can be well examined in the experiment. Accordingly, infrared heating is a very powerful tool in studying the reaction kinetics of brazing. The purpose of this investigation is focused in infrared brazing Ti–6Al–4V and Nb using the Ti–15Cu–15Ni foil. Both microstructure and reaction sequence of the brazed joint are extensively studied.

2. Experimental procedures

The base metals used in the experiment were Ti–6Al–4V plates and Nb rods. Both were machined into the dimension of 10 mm × 10 mm × 3 mm. Ti–15Cu–15Ni (wt%) foil with the

* Corresponding author. Tel.: +886 2 33664533; fax: +886 2 23634562.
E-mail address: rkshiue@ntu.edu.tw (R.K. Shiue).

0921-5093/$ – see front matter © 2006 Elsevier B.V. All rights reserved.
doi:10.1016/j.msea.2006.11.058

thickness of 50 μm and 50 mm wide was used as the brazing filler metal. Infrared brazing was carried out in a vacuum of 5×10^{-3} Pa at 970 °C for 180–3600 s, respectively. The heating rate of infrared brazing was kept at 10 °C/s throughout the experiment, and the average cooling rate between 570 and 1000 °C is roughly 1.3 °C/s. All infrared brazed specimens were preheated at 600 °C for 600 s.

The cross-section of the brazed specimens was examined using a LEO 1530 field emission scanning electron microscope (FESEM) equipped with an energy dispersive spectrometer (EDS). Its accelerating voltage was kept at 20 kV and minimum spot size of 1 μm. Quantitative chemical analysis was performed using a JEOL JXA 8200 superprobe with a minimum spot size of 1 μm. A Rigaku RINT 2100 X-ray diffractometer (XRD) was applied for structure analysis of selected infrared brazed specimens. The Cu Kα was chosen as the X-ray source, and its scan rate was set at 4°/min with the scan range between 30° and 90°. The X-ray diffraction pattern was recorded and identified based on the powder diffraction file (PDF).

Shear tests were performed in order to evaluate the bonding strength of selected brazed specimens [12–15]. A Shimadzu AG-10 universal testing machine with a constant speed of 0.5 mm/min compressed the brazed specimens. Cross-sections of above fractured specimens were mounted in an epoxy, and inspected using an SEM in order to locate the crack site of the joint.

3. Results and discussion

Fig. 1 shows the FESEM backscattered electron image (BEI) and EDS chemical analysis results of the joint infrared brazed at 970 °C for 180 s. At least three distinct regions are observed in the figure as marked by A, C and D, respectively. The region B shows transition from region A to region C. Ti–15Cu–15Ni foil is readily melted during infrared brazing due to the disappearance of original clad layers in the figure. The dissolution of both Ti–6Al–4V and Nb substrates into the molten braze is demonstrated by EPMA chemical analysis results of points 3–6 in the figure. It is noted that the Nb substrate is not reacted with Cu and Ni in the molten braze. In contrast, the Ti-rich phase is alloyed with Nb to form (βTi, Nb) close to the interface between the braze alloy and Nb substrate as marked by 6 in Fig. 1. Both Cu and Ni are reacted with Ti and form Ti_2Cu and Ti_2Ni as marked by 5. Additionally, the chemical composition of Cu and Ni is decreased from point 5 to points 4, 3 and 1, and they are depleted from the joint during brazing via diffusion from the braze alloy into Ti–6Al–4V substrate only.

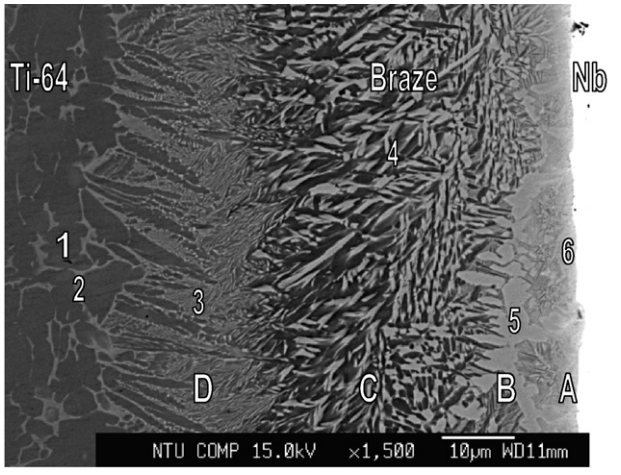

Location (phase), at%	Ti	Al	V	Cu	Ni	Nb
1 (α-Ti)	86.6	11.1	2.1	0.1	0.1	0.0
2 (β-Ti)	77.6	7.1	7.7	1.7	5.8	0.0
3 (Ti-rich)	82.4	5.8	2.4	4.7	4.4	0.2
4 (Ti-rich)	85.3	1.0	0.2	6.4	6.0	1.0
5 (Ti_2Cu, Ti_2Ni)	67.1	0.4	0.1	17.1	14.2	1.1
6 (βTi,Nb)	77.3	1.2	0.3	5.3	5.5	10.4

Fig. 1. The SEM BEI and EPMA chemical analysis results of the joint infrared brazed at 970 °C for 180 s using the Ti–15Cu–15Ni braze alloy.

The transformation of β-Ti upon cooling cycle of brazing significantly complicates microstructures of the brazed joint in using the Ti-based braze alloy [9,10,12]. It is crucial to grasp the reaction kinetics of the brazed joint prior to use such filler metals in confidence. Cu–Ni–Ti ternary alloy phase diagrams are cited here in order to unveil microstructural evolution of the infrared brazed joint. Fig. 2(a) shows the liquidus projection of Cu–Ni–Ti phase diagram, and the chemical composition of Ti–15Cu–15Ni braze alloy is marked by point A in the figure [16]. According to Fig. 2(a) and (b), solidification of the molten braze experiences a eutectic reaction at 900 °C upon cooling cycle of brazing:

$$L = Ti_2Cu + Ti_2Ni + \beta\text{-Ti} \quad (1)$$

The infrared brazed joint consists of Ti_2Cu, Ti_2Ni and β-Ti upon further cooling from 900 to 800 °C as illustrated in Fig. 2(c) and (d). It is noted that there are two Ti phases, Ti(HT) and Ti, in the Ti end of Cu–Ni–Ti isothermal sections due to the presence of two allotropic forms of Ti. In Fig. 2, Ti(HT) stands for the β-Ti, and Ti is the α-Ti. Fig. 2(e) demonstrates another important invariant reaction at 780 °C [16]:

$$Ti_2Cu + \beta\text{-Ti} = Ti_2Ni + \alpha\text{-Ti} \quad (2)$$

Based on the Eq. (2), the consumption of Ti_2Cu and β-Ti yields Ti_2Ni and α-Ti. Fig. 2(f) shows the Ti end of the Cu–Ni–Ti isothermal section at 700 °C, and the brazed joint consists of α-Ti, Ti_2Cu and Ti_2Ni.

The presence of equilibrium phases can be predicted from these phase diagrams. However, the morphology of various phases in the joint cannot only be determined from the phase diagram. The transformation kinetics always plays a crucial role in determine final microstructure of the joint for many Ti alloys. For instance, the redistribution of Cu, Ni (from the braze alloy), Al, V (from the Ti–6Al–4V substrate) and Nb (from the Nb substrate) in the infrared brazed joint greatly changes the transformation of β-Ti upon cooling cycle of the brazing. The Al element is the only α stabilizer for the Ti alloy among these elements. All other elements such as Cu, Ni, V and Nb are β stabilizers of the Ti alloy [2,3]. Cu–Ti and Ni–Ti are categorized as the β eutectoid system. In contrast, V and Nb in Ti belong to

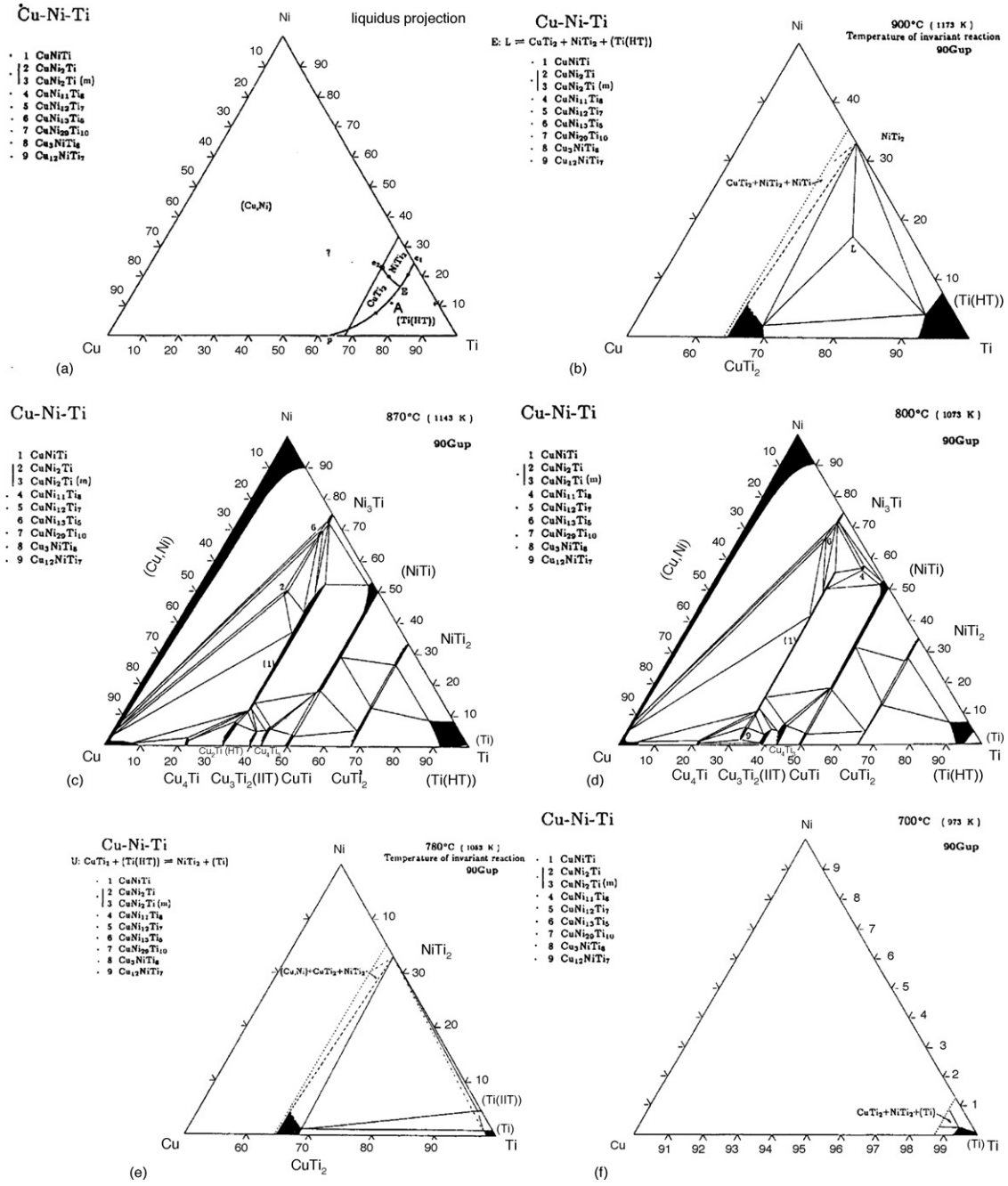

Fig. 2. Cu–Ni–Ti ternary alloy phase diagrams: (a) liquidus projection and isothermal section at (b) 900 °C (invariant reaction), (c) 870 °C, (d) 800 °C, (e) 780 °C (invariant reaction), (f) 700 °C [16].

the β isomorphous system. Accordingly, it is possible that the β-Ti is stabilized at room temperature by alloying Nb and V.

Cross-sections of A, B, C and D regions in Fig. 1 are cut and polished in order to be inspected in greater depth. Fig. 3 shows XRD, SEM BEIs and EDS chemical analysis results in atomic percent of the cross-section at the location A in Fig. 1. The infrared brazed joint consists of (βTi, Nb) matrix, Ti_2Cu and Ti_2Ni phases based on the XRD structural analysis. According to the Nb–Ti binary alloy phase diagram, the maximum solubility of Nb in α-Ti is about 2 at.%, and the β-Ti can be stabilized by alloying Nb above 38 at.% at 400 °C [17]. The Nb content of (βTi, Nb) is 17.5 at.% as marked by 3 in Fig. 3. It is expected that both α and β-Ti coexist at location A as proven by the XRD analysis.

Fig. 4 displays XRD, SEM BEIs and EDS chemical analysis results of the cross-section at the location B in Fig. 1. The microstructure of Fig. 4 is different from that of Fig. 3. α-Ti (point 5), transformed β (points 2 and 4), Ti_2Cu and Ti_2Ni (points 1 and 3) are identified from the XRD analysis. The terminology of transformed β-Ti has been used here. The transformed β-Ti phase as marked by 2 and 4 with the Cu and Ni contents of 8.6 at.% will be discussed later. However, the β-Ti is absent from

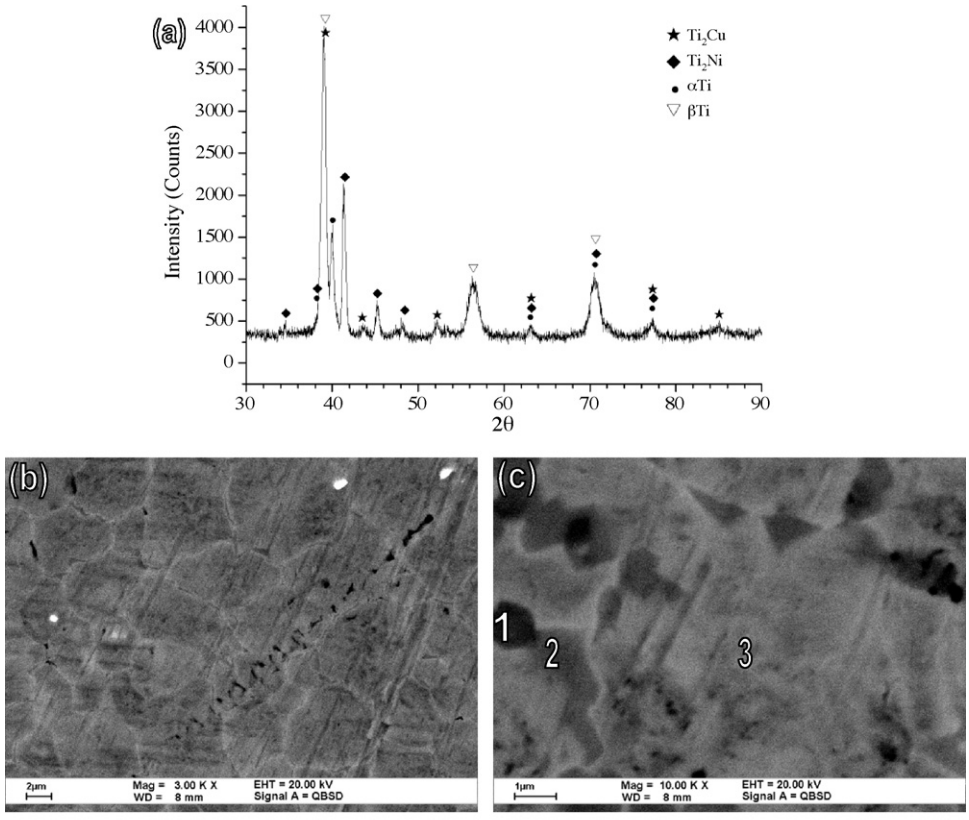

Location (phase) / at%	Al	Nb	Ti	V	Ni	Cu
1 (Ti_2Cu, Ti_2Ni)	1.1	8.6	65.4	0.0	18.4	6.7
2 (Ti_2Cu, Ti_2Ni)	0.5	8.4	64.7	0.0	11.5	14.9
3 (βTi,Nb)	0.8	17.5	74.4	0.0	4.2	3.2

Fig. 3. (a) XRD, (b and c) SEM BEIs and EDS chemical analysis results of the cross-section at location A shown in Fig. 1.

the XRD analysis result because of low Nb displayed in Fig. 4. It is worth mentioned that both Ti_2Cu and Ti_2Ni phases are difficult to be distinguished in the SEM BEIs due minor difference in atomic number between Cu and Ni. According to Eq. (1), the eutectic melt is solidified into β-Ti, Ti_2Cu and Ti_2Ni phases, so dendritic grain boundary Ti_2Cu and Ti_2Ni phases are widely observed in Fig. 4. Additionally, Ti_2Cu and Ti_2Ni are observed not only along the grain boundaries but also in the prior β-Ti grains as illustrated in the figure.

As described earlier, the transformation of β-Ti upon cooling cycle of brazing significantly complicates microstructure of the joint. The β-Ti dissolves huge amount of β stabilizers, Cu, Ni and Nb. However, solubilities of these β stabilizers are greatly decreased in α-Ti. The transformation of β-Ti into α-Ti is greatly influenced by the presence of alloying elements in Ti. Depending on the rate of forming eutectoid, alloying elements in the Ti alloy are classified as active and sluggish eutectoid formers. Both Cu and Ni additions in the Ti alloy are generally classified as active eutectoid formers, i.e., the Cu, Ni alloyed Ti with rapid eutectoid decomposition [18]. Wells [19] studied the microstructural evolution of Cu diffusion bonded pure Ti. The microstructures of these joints varied from pearlite-like for the 6% Cu content specimen to a bainite-like structure for the 9.5% Cu content one [19]. There is no pearlite-like phase found in Fig. 4, and the transformed β-Ti is similar to the bainite-like phase in the study. In Fig. 4, points 2 and 4 are transformed β-Ti, which is obtained from the transformation of β-Ti upon cooling cycle of brazing. A black α-Ti phase is found as marked by 5 featured with low Cu, Nb and Ni concentrations, and it is consistent with the invariant reaction at 780 °C as described in Eq. (2). The β-Ti reacts with Ti_2Cu, and forms α-Ti and Ti_2Ni.

Fig. 5 displays XRD, SEM BEIs and EDS chemical analysis results in atomic percent of the cross-section at location C in Fig. 1. The amount of grain boundary Ti_2Cu and Ti_2Ni phase is decreased. It is resulted from the depletion of both Cu and Ni contents from the braze alloy. Based on Cu–Ti and Ni–Ti binary alloy phase diagrams, the maximum solubilities of Cu and Ni in β-Ti are 13.5 and 10 at.%, respectively [17]. Diffusion of both Cu and Ni from the molten braze into the Ti–6Al–4V substrate is driven by concentration gradient during brazing [19,20]. Additionally, dissolution of the Ti–6Al–4V substrate into the molten braze also dilutes concentrations of Cu and Ni in the braze alloy. Decreasing Cu and Ni contents from the braze alloy during infrared brazing results in less eutectic grain boundary Ti_2Cu and Ti_2Ni intermetallics. On the other hand, the eutectoid decomposition of β-Ti is widely observed in the prior β-Ti grains

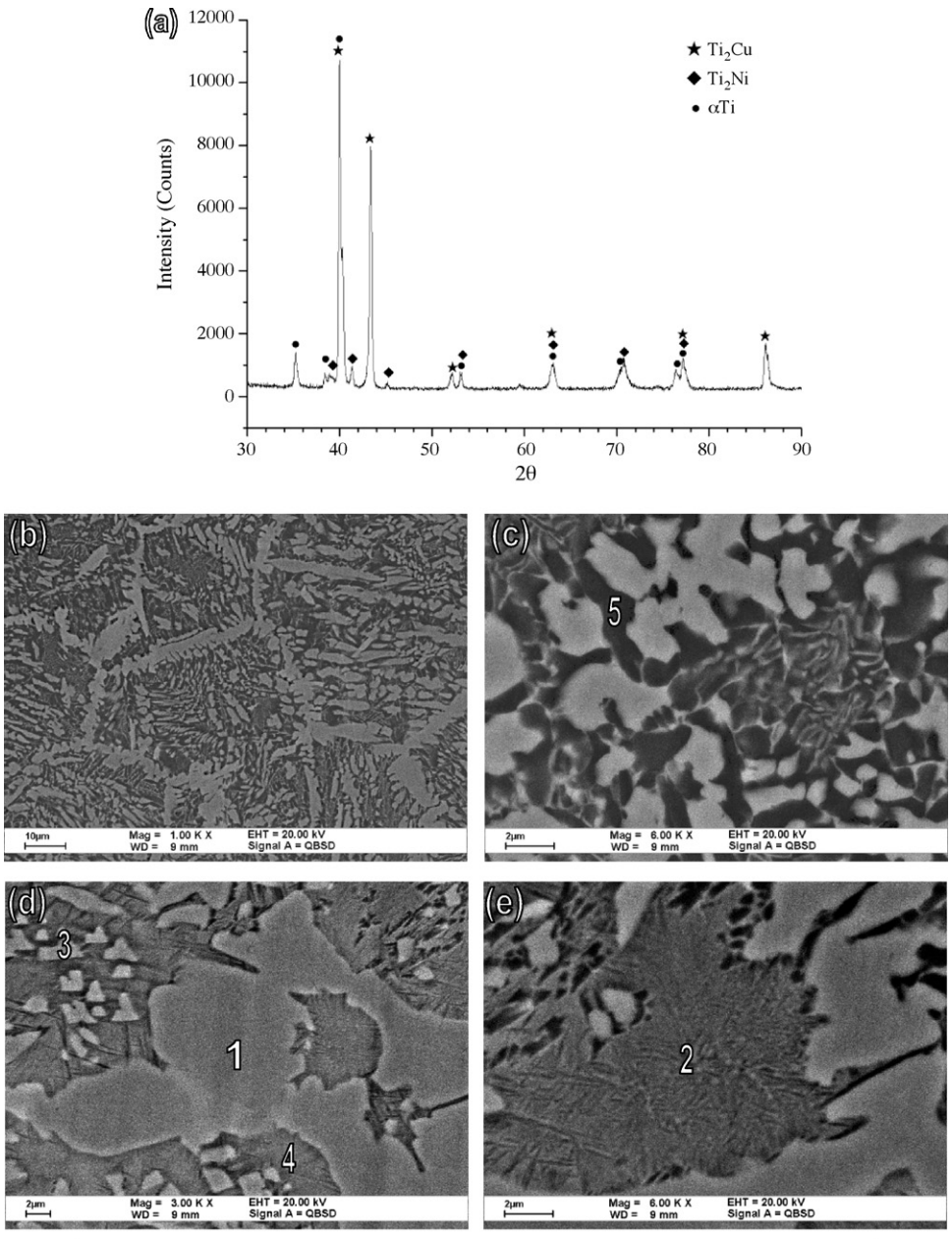

Location (phase) / at%	Al	Nb	Ti	V	Ni	Cu
1 (Ti_2Cu, Ti_2Ni)	0.8	1.3	64.9	0.0	13.5	19.5
2 (transformed β-Ti)	3.3	6.2	81.8	0.1	5.3	3.3
3 (Ti_2Cu, Ti_2Ni)	1.2	2.1	67.0	0.0	13.4	16.4
4 (transformed β-Ti)	2.9	6.4	82.2	0.0	5.3	3.3
5 (α-Ti)	2.2	1.6	92.1	0.0	2.4	1.7

Fig. 4. (a) XRD, (b–e) SEM BEIs and EDS chemical analysis results of the cross-section at location B shown in Fig. 1.

as illustrated in Fig. 5. The decomposed β-Ti yields mixture of α-Ti, Ti_2Cu and Ti_2Ni as demonstrated by the XRD analysis.

Fig. 6 displays XRD and SEM BEIs of the cross-section at location D as shown in Fig. 1. The EDS chemical analysis of separate phase cannot be accurately performed due to limited lateral resolution of SEM. The thickness of clad foil is 50 μm, and the dissolution of Ti–6Al–4V substrate into the molten braze is confined due to rapid thermal history of infrared brazing at 970 °C for 180 s. The kinetic path in region D is different from that in regions A–C, and only solid-state interdiffusion of solutes in β-Ti is proceeded during brazing. Coarse eutectic grain boundary Ti_2Cu and Ti_2Ni intermetallics are not available since there is no solidification of the residual melt in region D. The microstructure of entire region is caused by decomposition of original β-Ti alloyed with Cu and Ni after infrared brazing. Consequently, a much finer eutectoid mixture of Ti_2Cu, Ti_2Ni and α-Ti is

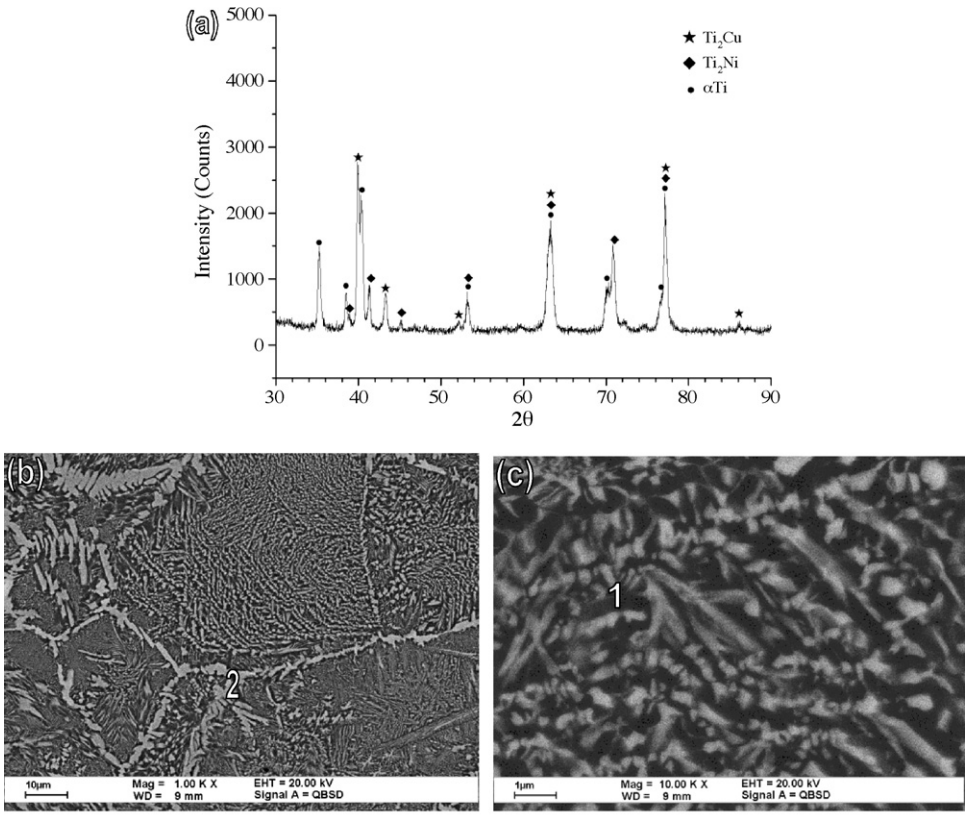

Location (phase)	Al	Nb	Ti	V	Ni	Cu
1 (Ti-rich)	5.0	0.3	88.3	0.0	3.8	2.5
2 (Ti_2Cu, Ti_2Ni)	1.6	0.2	67.6	0.0	11.9	18.7

Fig. 5. (a) XRD, (b and c) SEM BEIs and EDS chemical analysis results of the cross-section at location C shown in Fig. 1.

observed in Fig. 6 as compared with those in Figs. 4 and 5. Both lamellar and non-lamellar eutectoid mixture are found in region D. It has been reported that the eutectoid morphology is non-lamellar in the hypoeutectoid alloys and lamellar in the near eutectoid alloys for the Ti–Ni system [18]. The eutectoid composition of Ti–Ni binary phase diagram is 4.5 at.%, and the Ni concentration in region D is 4.4 at.% as marked by 3 in Fig. 1. It is consistent with the previous study.

Fig. 7(a) shows SEM cross-section of the joint infrared brazed at 970 °C for 600 s. The microstructure of Fig. 7(a) is different from that of Fig. 1. The coarse eutectic grain boundary Ti_2Cu and Ti_2Ni have been replaced by fine eutectoid mixture of Ti_2Cu, Ti_2Ni and transformed β-Ti. Fig. 7(b) and (c) displays SEM BEI, XRD and EDS chemical analysis results of the cross-section at location E in Fig. 7(a). Based on the XRD structural analysis result, retained β-Ti is also identified in region E. It is resulted from high Nb content of the β-Ti as demonstrated by EDS chemical analysis in the figure.

With increasing the brazing time, the original chemical composition of Ti–15Cu–15Ni as marked by A in Fig. 2(a) moves towards to Ti end of the ternary phase diagram. According to the previous studies, Ti_2Cu and Ti_2Ni are not stable phases at the brazing temperature of 970 °C [12]. Increasing the brazing temperature and/or time result in decreasing amounts of Ti_2Cu and Ti_2Ni, which are eventually disappeared from the Ti-rich matrix [12,13]. In other words, depleting the melting point depressants, Cu and Ni, from Ti–15Cu–15Ni braze alloy is persistent during infrared brazing. Additionally, dissolution of both Ti–6Al–4V and Nb substrates also results in dilution of Cu and Ni concentrations in the molten braze. Isothermal solidification of the molten braze is proceeded during brazing, and it renders β-Ti alloyed with various amounts of Cu, Ni, V and Nb at the brazing temperature. The β-Ti subsequently experiences eutectoid decomposition upon the cooling cycle of brazing, and it yields Ti_2Cu, Ti_2Ni, transformed β and retained β phases as marked by E in Fig. 7. The average cooling rate after infrared brazing is kept at 1.3 °C/s throughout the experiment, so redistribution of solutes (Cu, Ni and Nb) in the β-Ti plays a crucial role in determining final microstructure of the joint. Accordingly, the morphology of transformed β-Ti is changed from location E to F due to lower Cu, Ni and Nb concentrations at location F.

Fig. 8(a) shows SEM cross-section and EPMA chemical analysis results of the joint infrared brazed at 970 °C for 3600 s. The microstructure of Fig. 8(a) is significantly different from those of Figs. 1 and 7(a). The eutectoid mixture of Ti_2Cu, Ti_2Ni and transformed β-Ti are completely disappeared from region G in Fig. 8(a). Based on the EPMA analysis across the joint (Fig. 8(b)), the chemical composition at location G is alloyed with high concentration of Nb, a strong β stabilizer of Ti. Because the β-Ti is stabilized by Nb, decomposition of

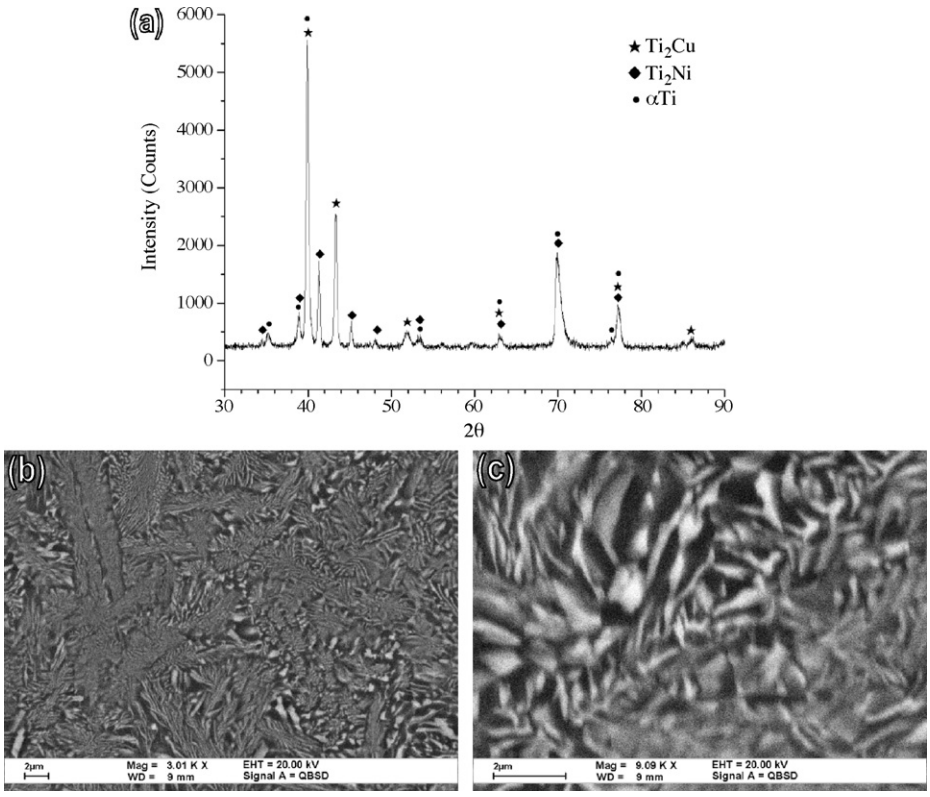

Fig. 6. (a) XRD, (b and c) SEM BEIs of the cross-section at location D shown in Fig. 1.

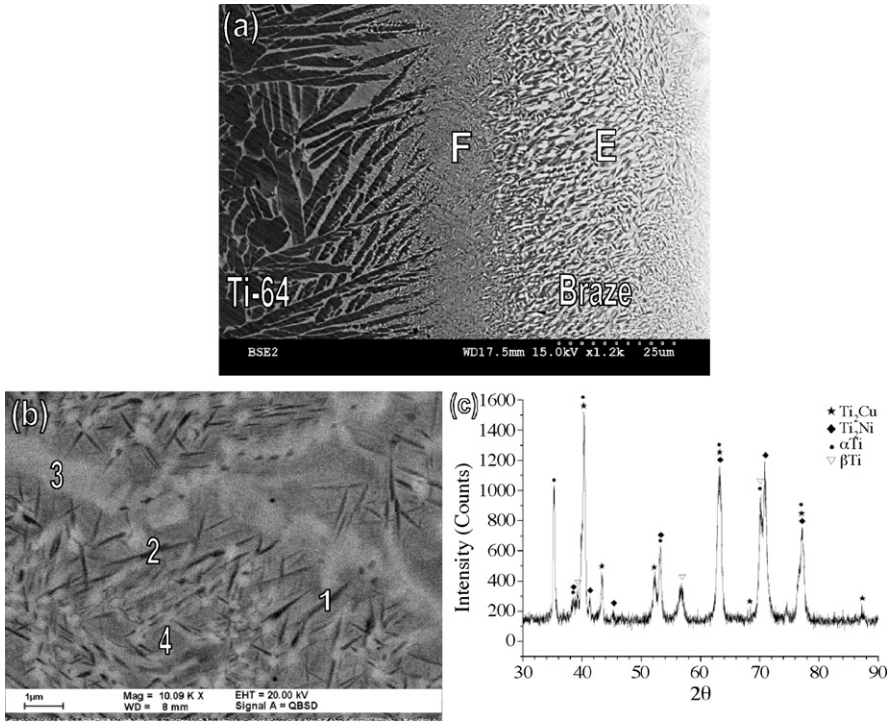

Location (phase)) / at%	Al	Nb	Ti	V	Ni	Cu
1 (transformed β-Ti)	3.3	10.2	76.2	0.2	5.0	5.1
2 (transformed β-Ti)	3.1	10.1	76.6	0.0	4.7	5.5
3 (Ti_2Ni, Ti_2Cu)	2.5	6.4	67.4	0.0	17.0	6.6
4 (transformed β-Ti)	4.2	11.1	77.2	0.1	4.2	3.2

Fig. 7. (a) SEM BEI cross-section of the joint infrared brazed at 970 °C for 600 s, (b and c) SEM BEI, XRD and EDS chemical analysis results of the cross-section at location E in (a).

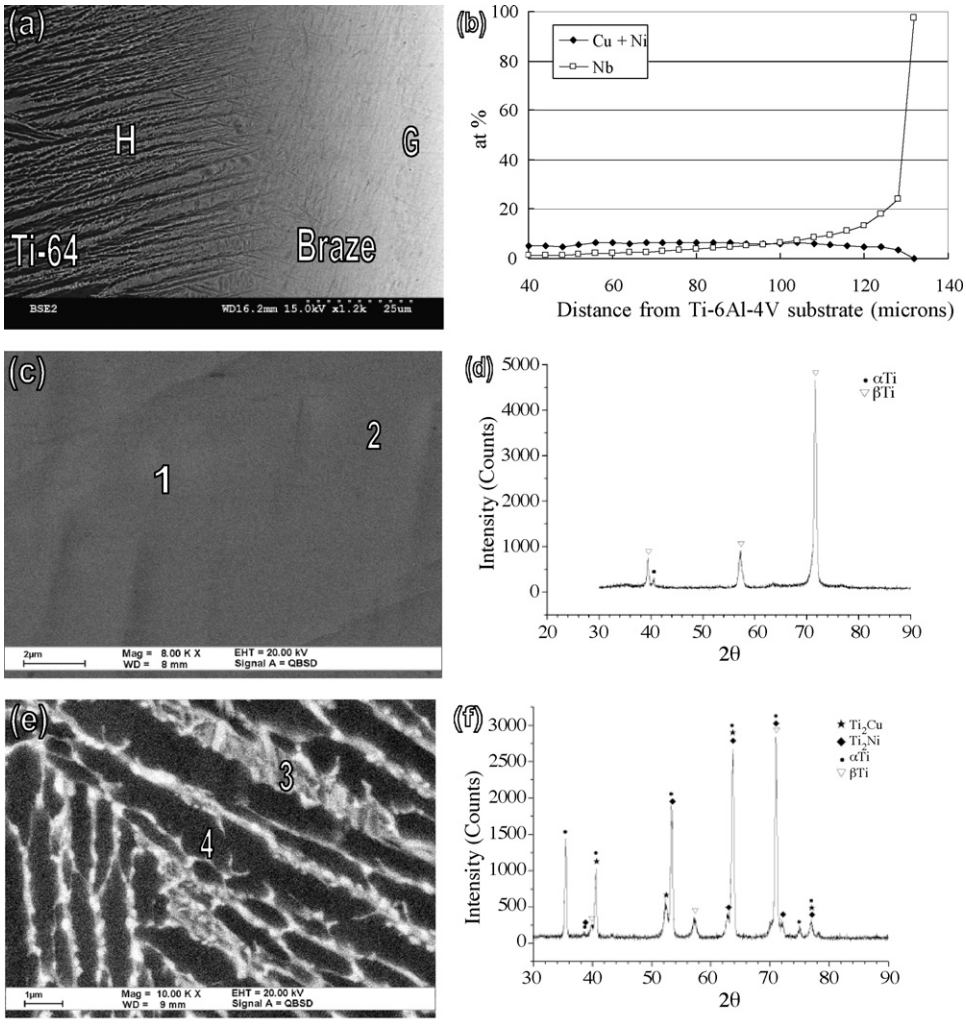

Location (phase)) /at%	Al	Nb	Ti	V	Ni	Cu
1 (βTi,Nb)	5.2	13.8	75.5	0.4	2.3	3.0
2 (βTi,Nb)	5.1	15.2	71.7	1.0	3.1	3.9
3 (β-Ti)	8.4	1.2	78.0	4.5	4.1	3.9
4 (α-Ti)	10.4	0.6	85.2	1.0	1.0	1.7

Fig. 8. (a) SEM cross-section, (b) EPMA chemical analysis results of the joint infrared brazed at 970 °C for 3600 s, (c and d) XRD, SEM BEI and EDS chemical analysis results of the cross-section at location G in (a), (e and f) XRD, SEM BEI and EDS chemical analysis results of the cross-section at location H in (a).

the β-Ti is not available in this region. Ti_2Cu, Ti_2Ni and transformed β phases are not observed anymore as illustrated in Fig. 8(c). Fig. 8(d) displays the XRD structural analysis of the cross-section at location G in Fig. 8(a). The brazed joint at location G mainly consists of β-Ti stabilized by alloying high Nb concentration as marked by 1 and 2 in Fig. 8(c).

It is also noted that coarse acicular α-Ti is observed at the interface close to Ti–6Al–4V substrate as illustrated in Fig. 8(a). In contrast, the microstructure of Ti–6Al–4V base metal is typically comprised of equiaxed α and intergranular β (Figs. 1 and 7(a)). The formation of large acicular α is also related to Ti–6Al–4V substrate alloyed with Cu and Ni [19]. Compared among Figs. 1, 7(a) and 8(a), the interfacial acicular α-Ti is greatly coarsened with increasing the brazing time due to the growth of prior β-Ti grains at the brazing temperature.

Fig. 8(e) shows SEM BEI cross-section at location H in Fig. 8(a), and both β-Ti and acicular α-Ti are observed as marked by 3 and 4 in the figure. Based on the XRD result shown in Fig. 8(f), Ti_2Cu and Ti_2Ni are also identified from the analysis. It is deduced that the white spots inside the β-Ti in Fig. 8(e) are Ti_2Cu and Ti_2Ni phases. However, chemical analyses of these spots cannot be performed accurately due to limited lateral resolution of the EDS analysis.

Fig. 9 shows SEM images displaying cross-sections and fractographs of infrared brazed joints after shear tests. It is obvious that all specimens are fractured along the Nb substrate, and dimple dominated fracture is widely observed on fractographs. Based on this information, the use of Ti–15Cu–15Ni filler metal demonstrates great potential in brazing Ti–6Al–4V and Nb.

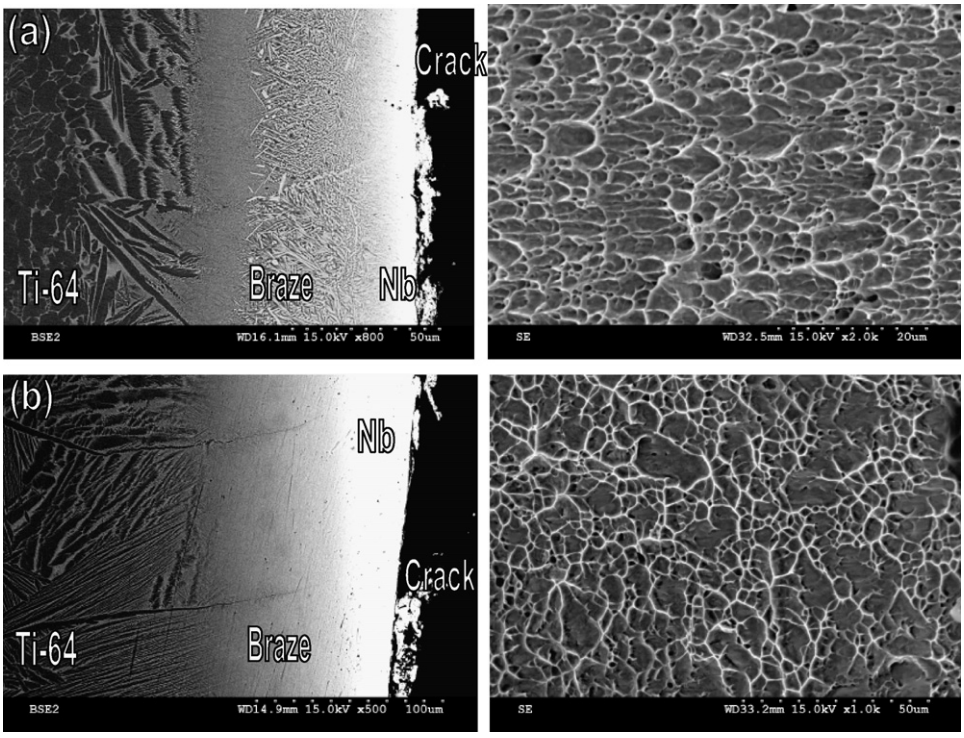

Fig. 9. SEM images displaying cross-sections and fractographs of joints infrared brazed at 970 °C for (a) 600 s and (b) 3600 s after shear tests.

4. Conclusions

Infrared vacuum brazing of Ti–6Al–4V and Nb metal using the Ti–15Cu–15Ni braze alloy has been accessed in the experiment. Important conclusions are summarized below:

1. The microstructural evolution of infrared brazed joint is primarily depended upon redistribution of alloying elements such as Cu, Ni and Nb across the joint. For the specimen infrared brazed at 970 °C for 180 s, the microstructure of the joint changes from coarse eutectic Ti_2Cu, Ti_2Ni and transformed β-Ti at center into eutectoid mixture of decomposed β-Ti close to the Ti–6Al–4V substrate.
2. Increasing the brazing time results in decreasing Ti_2Cu and Ti_2Ni, which are eventually disappeared from the Ti matrix. It is resulted from depletion of both Cu and Ni from the braze alloy into Ti–6Al–4V substrate. Isothermal solidification instead of eutectic solidification of the molten braze is proceeded in brazing. Accordingly, the microstructure of the infrared brazed joint with longer brazing time, e.g. 600 s, is free of coarse eutectic grain boundary Ti_2Cu and Ti_2Ni intermetallic compounds. Fine eutectoid microstructure dominates the entire joint due to decomposition of the β-Ti upon cooling cycle of brazing.
3. For the specimen infrared brazed for 3600 s, Ti_2Cu, Ti_2Ni and transformed β phases are replaced by the β-Ti stabilized by alloying high concentration of Nb. The Nb substrate does not react with Cu and Ni in the braze alloy, but it is primarily alloyed with the Ti. Additionally, the size of acicular α at the interface close to Ti–6Al–4V substrate is significantly increased with increasing the brazing time.
4. Infrared brazed specimens are fractured along the Nb substrates, and dimple dominated fracture is widely observed on fractographs. The application of Ti–15Cu–15Ni filler metal demonstrates great potential in brazing Ti–6Al–4V and Nb.

Acknowledgements

The authors gratefully acknowledge the financial support of this study by National Science Council (NSC), Republic of China under NSC grant 95-2221-E-002-057.

References

[1] J.R. Davis, Metals Handbook, Properties and Selection: Nonferrous Alloys and Special Purpose Materials, vol. 2, ASM International, Materials Park, 1990.
[2] R. Roger, E.W. Collings, G. Welsch, Materials Properties Handbook: Titanium Alloys, ASM International, Materials Park, 1993.
[3] W.F. Smith, Structure and Properties of Engineering Alloys, McGraw-Hill, New York, 1993.
[4] D.W. Liaw, R.K. Shiue, Metall. Mater. Trans. 36A (2005) 2415–2427.
[5] D.L. Olson, T.A. Siewert, S. Liu, G.R. Edwards, ASM Handbook Welding, Brazing and Soldering, vol. 6, ASM International, Materials Park, 1993.
[6] M. Schwartz, Brazing for the Engineering Technologist, ASM International, Materials Park, 1995.
[7] M. Schwartz, Brazing, ASM International, Materials Park, 1987.
[8] G. Humpston, D.M. Jacobson, Principles of Soldering and Brazing, ASM International, Materials Park, 1993.
[9] I.T. Hong, C.H. Koo, Int. Refrac. Met. H. M. 24 (2006) 247–252.
[10] I.T. Hong, C.H. Koo, Mater. Chem. Phys. 94 (2005) 131–140.
[11] C.S. Chang, B. Jha, Weld. J. 82 (2003) 28.
[12] C.T. Chang, Y.C. Du, R.K. Shiue, C.S. Chang, Mater. Sci. Eng. 420A (2006) 155–164.
[13] C.T. Chang, R.K. Shiue, C.S. Chang, Scr. Mater. 54 (5) (2006) 853–858.

[14] R.K. Shiue, S.K. Wu, C.H. Chan, C.S. Huang, Metal. Mater. Trans. 37A (2006) 2207–2217.
[15] R.K. Shiue, S.K. Wu, C.H. Chan, J. Alloy. Comp. 372 (2004) 148–157.
[16] P. Villars, A. Prince, H. Okamoto, Handbook of Ternary Alloy Phase Diagrams, ASM International, Materials Park, 1995.
[17] T.B. Massalski, Binary Alloy Phase Diagrams, ASM International, Materials Park, 1990.
[18] S. Krishnamurthy, F.H. Froes, Int. Mater. Rev. 34 (1989) 297–311.
[19] R.R. Wells, Weld. J. 55 (1) (1976) 20s–27s.
[20] C.T. Chang, R.K. Shiue, C.S. Chang, Proceedings of the Third International Brazing & Soldering Conference, San Antonio, Texas, 2005.